Decreased Medial Temporal Oxygen Metabolism in Alzheimer's Disease Shown by PET

Kazunari Ishii, Hajime Kitagaki, Michio Kono and Etsuro Mori

Divisions of Neuroimaging Research and Radiology Service, Clinical Neurosciences and Neurology Service, Hyogo Institute for Aging Brain and Cognitive Disorders, Himeji, and Department of Radiology, Kobe University School of Medicine, Kobe, Japan

In mild-to-moderate Alzheimer's disease, previous PET studies failed to reveal significant involvement in the medial temporal lobe having pathologically neurodegenerative changes. The purpose of this study was to clarify the medial temporal perfusion and functional changes in mild-to-moderate Alzheimer's disease using PET. **Methods:** Sixteen patients with probable mild-to-moderate Alzheimer's disease (age 62.9 ± 6.0 yr, MMSE 17.7 ± 3.7) and 14 normal volunteers (age 60.9 ± 5.9 yr) were studied. Regional cerebral blood flow (CBF), oxygen metabolism ($CMRO_2$) and oxygen extraction fraction (OEF) were measured using ^{15}O steady-state method and PET. By rendering magnetic resonance volumetry of the medial temporal structures, the significance of partial volume effects on PET study measurements was examined. **Results:** The mean $CMRO_2$ in the medial temporal, as well as in the parietal and lateral temporal cortices were significantly lower in the patient group than in the control group. The mean CBF in the parietal and lateral temporal cortices also significantly decreased in the patient group. The OEF in the medial temporal was also decreased in the Alzheimer's disease group, while the OEF in the other cortical regions in Alzheimer's disease group were similar to that of control group. Decline of medial temporal oxygen consumption was the most distinctive feature of Alzheimer's disease. Those measurements were independent from volume of medial temporal structures. In Alzheimer's disease, medial temporal $CMRO_2$ and CBF correlated with some of the nonverbal memory test scores and cognitive impairment scales, when normalized for individual difference. **Conclusion:** Medial temporal oxygen metabolism was markedly affected in patients with mild-to-moderate Alzheimer's disease. This measure substantiated the functional impairment of the medial temporal region in Alzheimer's disease.

Key Words: PET; medial temporal lobe; cerebral blood flow; cerebral oxygen metabolism; Alzheimer's disease

J Nucl Med 1996; 37:1159–1165

Alzheimer's disease is the largest constituent of degenerative dementias. Characteristically, the disease starts with impairment of memory followed by multiple domains of cognitive dysfunction. The medial temporal lobe, including the hippocampus, which provides an anatomical substrate for memory function, is a site invariably and centrally affected in Alzheimer's disease patients (*1,2*). PET and SPECT provide information about cerebral function. These techniques have demonstrated decreased regional glucose metabolism and blood flow in the posterior temporal and parietal lobes, which are also primarily involved in Alzheimer's disease, in studies of Alzheimer's disease (*3–9*). Frackowiak et al. (*3*) reported decreased cerebral blood flow (CBF) and cerebral metabolic rate for oxygen ($CMRO_2$) in the parietal lobes in patients with degenerative dementia. Nybäck et al. (*4*) and Friedland et al. (*6*) both demonstrated parietal or parietotemporal glucose hypometabolism in a patient with Alzheimer's disease. Fukuyama et al. (*10*) reported significant reduction in CBF, $CMRO_2$ and cerebral metabolic ratio of glucose (CMRGlu), more in the last, in posterior parietal cortex in patients with Alzheimer's disease. It is also pointed out that parietal or parietotemporal hypoperfusion and hypometabolism have only a limited role in distinguishing Alzheimer's disease from normal aging and other diseases. Powers et al. (*11*) studying the accuracy of $H_2{}^{15}O$ PET for the diagnosis of Alzheimer's disease, reported a sensitivity of 38% and a specificity of 88% for identifying patients with probable Alzheimer's disease in a heterogeneous group of normal and demented elderly.

Memory and the medial temporal lobe, including the hippocampus and parahippocampal gyrus, should be a central focus of studies of Alzheimer's disease patients. In the neuroradiological field, volumetric studies using magnetic resonance (MR) imaging have indicated structural changes of the hippocampus in Alzheimer's disease, and the role of hippocampal atrophy in the diagnosis of Alzheimer's disease has been delineated (*12–14*). Only a few functional imaging studies, however, have addressed the hippocampus or medial temporal region. Nybäck et al. (*4*) failed to demonstrate a difference of hippocampal glucose metabolism between patients with Alzheimer's disease and normal controls, and Cutler et al. (*5*) reported inconsistent results such as relative preservation or increased glucose metabolism in the hippocampus to the whole brain despite low absolute glucose metabolism in patients with advanced Alzheimer's disease. Although Ohnishi et al. (*15*) used ^{99m}Tc-HMPAO and SPECT and found that hippocampal "hypoperfusion" in Alzheimer's disease and partial volume effects could not be eliminated because of the limited spatial resolution of SPECT and the reduced bulk of the hippocampus in Alzheimer's disease. A possible limitation of such studies is in its small size that is much greater than the spatial resolution of PET or SPECT.

By evaluating blood flow and oxygen metabolism with PET and ^{15}O steady-state technique (*16*), we sought to elucidate functional impairment and pathophysiological feature of the medial temporal lobe in patients with Alzheimer's disease. In addition, we investigated the clinical significance of medial temporal metabolic and perfusional changes for the diagnosis of Alzheimer's disease.

MATERIALS AND METHODS

Subjects

We studied 30 subjects, including 16 patients with Alzheimer's disease (13 women, 3 men; aged 62.9 ± 6.0) and 14 sex-, age-matched healthy volunteers (mean ± s.d. aged 60.9 ± 5.9, 11 women, 3 men; aged 60.9 ± 5.9 yr). According to the following criteria, patients with Alzheimer's disease were selected from those who were admitted in our hospital for examination between

Received Aug. 14, 1995; revision accepted Nov. 15, 1995.

For correspondence or reprints contact: Kazunari Ishii, MD, Division of Neuroimaging Research, Hyogo Institute for Aging Brain and Cognitive Disorders, 520 Saisho-Ko, Himeji, 670, Japan.

TABLE 1
Patients' Characteristics

Patient no.	Age (yr)	Sex	MMSE	ADAS
1	53	M	18	20
2	54	M	21	19
3	55	M	21	29
4	56	F	23	10
5	58	F	21	15
6	62	F	18	15
7	63	F	16	26
8	63	F	17	35
9	64	F	13	40
10	65	F	16	26
11	67	F	11	47
12	68	F	22	20
13	68	F	15	18
14	69	F	18	19
15	69	F	21	16
16	72	F	12	35

MMSE = Mini-Mental State Examination; ADAS = Alzheimer's Disease Assessment Scale.

November 1993 and March 1995. All patients were examined by both neurologists and psychiatrists and underwent brain MRI, MR angiography of the neck and head, electroencephalography and standard neuropsychological examinations for more than 1 mo after admission. The inclusion criteria included:

1. National Institute of Neurological and Communicative Disorders and Stroke/Alzheimer's Disease and Related Disorders Association (NINCDS/ADRDA) criteria for probable Alzheimer's disease (*17*).
2. No evidence of focal brain lesions on MR images.
3. Functional severity mild-to-moderate: grades 1 and 2 on clinical dementia rating (*18*).
4. Age below 75 yr.

Exclusion criteria included:

1. Complication of other neurological diseases or ill physical conditions.
2. Presence of severe language, attention and behavioral disorders that would make a PET procedure difficult.
3. Lack of informed consent from patients and their relatives.

The mean Mini-Mental State Examination (MMSE) (*19*) score was 17.7 ± 3.7 and the mean Alzheimer's Disease Assessment Scale (ADAS) (*20*) score was 25.0 ± 9.7 (Table 1). The Alzheimer's disease patients were evaluated by the following memory tests: figural memory, logical memory, visual paired associates, verbal paired associates and visual reproduction scores of the Wechsler memory scale -Revised (WMS - R) (*21*).

Healthy volunteers (n = 14), who were recruited from social service clubs, were control subjects. They had no neurological signs or significant medical antecedents and no abnormal findings on MR images. Informed consent was obtained from all patients or their relatives and from all volunteers. The PET procedure was approved by our institution's ethical committee.

MRI

Before PET imaging, all subjects underwent MRI for diagnosis and anatomical reference. The MR scanner uses a circularly polarized head-coil as both transmitter and receiver. Sagittal, coronal and axial T1-weighted SE images (repetition time [TR] msec/echo time [TE] msec = 550/15, two excitations, 5 mm thickness, 2.5 mm gap) and axial T2-weighed fast SE images (3000/21,105, two excitations) were obtained. Three-dimensional spoiled gradient echo imaging (TR 14 msec, TE 3 msec, flip angle 20°, 1.5 mm thickness by 124 slices) was performed as a reference for posthoc anatomical analysis of PET and for volumetry of the medial temporal structures. The MR images were obtained 2–28 days before the PET examination.

Immediately before the PET examination, sagittal gradient-echo images (TR/TE = 60/2.9, 10 mm thickness) were obtained to determine the coordinates for positioning the head on the PET table. The subject's head attached with a head gear horizontally placed on the MR table. Three landmarks indicating the iso-center of the field of view were placed on the head gear. On the midsagittal section, the angle of the anterior commissure-posterior commissure (AC-PC) plane to the horizontal plane and the distance between the AC-PC plane and the iso-center of field of view were determined.

PET Procedure

PET images were obtained with a tomograph that has four rings located 13 mm apart and yields a transverse resolution of 4.5 mm FWHM (*22*). The slice thickness was 11 mm and the slice interval was 6.5 mm when the z-motion mode was used.

The gantry and scanner table were adjusted according to the coordinates determined by MRI so that scans were taken parallel to the AC-PC plane from 32.5 mm below to 52.0 mm above the AC-PC plane at 6.5-mm intervals. We chose the direct AC-PC plane scanning instead of orbito-meatal (OM) plane scanning to fit the stereotaxic atlas of Talairach and Tournoux (*23*) to avoid reslicing which may reduce the original spatial resolution.

Cross-calibration between the scanner and the well counter and the cross-planes of the scanner was obtained before each subject's study. A transmission scan was obtained using $^{68}Ga/^{68}Ge$ for absorption correction after subject positioning. PET studies were performed under resting conditions with eyes closed and ears unplugged. CO_2 and O_2 labeled with ^{15}O were continuously inhaled at 200 MBq/200 ml/min and 500 MBq/200 ml/min, respectively. Emission scans were obtained during inhalation of $C^{15}O_2$ and $^{15}O_2$ after equilibrium was reached (the equilibrium time was about 10 min) and confirmed with the head activity curve measured by the scanner's detector banks. The $C^{15}O$ emission scan started 2–3 min after a 1-min inhalation of 2000 MBq/200 ml $C^{15}O$. Imaging took 10 min for $C^{15}O_2$ and $^{15}O_2$ and 4 min for $C^{15}O$. Arterial blood sampling was performed from a catheter placed in the radial artery three times per each scan (at the start of the scan, midpoint of the scan and 30 sec before the end of the scan) to determine radioactivity and blood gas analysis. During the examination, head stability was monitored by a laser marker.

CBF, $CMRO_2$ and the oxygen extraction fraction (OEF) were calculated with the data obtained from the steady-state method using ^{15}O-labeled gases (*16*). Cerebral blood volume (CBV) was calculated by the 1-min inhalation of ^{15}O-labeled carbon monoxide and was incorporated in the correction of vascular space for $CMRO_2$ and OEF (*24*).

Data Analysis

PET and MR image datasets were directly transmitted to a workstation from the PET and MRI imaging units and analyzed using image analyzing software. MR images of identical three-dimensional scales and coordinates to the PET images were made for anatomical references to the PET analysis. Both PET and MR images were displayed side-by-side on a display monitor and two or three circular regions of interest (ROIs) 10 mm diameter were determined on the cortical ribbon of each region on the CBF image. Anatomical coordinates were verified on the corresponding MR image (Fig. 1). ROIs were then placed on the medial temporal lobe (hippocampus and parahippocampal gyrus), lateral temporal lobe

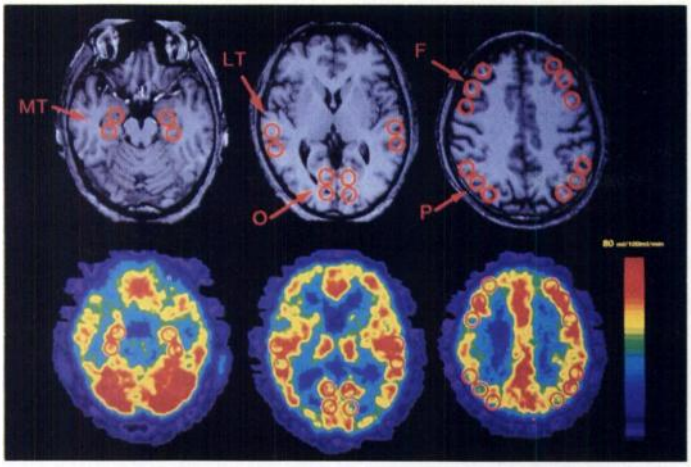

FIGURE 1. MR and CBF PET images of a normal control subject with overlayed ROIs. MT = medial temporal; LT = lateral temporal; O = occipital; F = frontal; and P = parietal cortex.

(superior and middle temporal gyri), occipital lobe (cuneus), frontal lobe (superior and middle frontal gyri), parietal lobe (supramarginal and angular gyri) and cerebellar cortices. The same ROIs were transferred to the OEF, $CMRO_2$ and cerebral blood volume images and regional OEF, $CMRO_2$, and CBV were measured, these value were shown as the average of the right and left regional values.

Hippocampal formation and parahippocampal gyrus volumes were measured on the original spoiled gradient echo MR images by using a segmentation technique along with tracing and thresholding (*25,26*). The threshold was set at a range between the minimum and maximum pixel values, in which the maximum value was the largest pixel value of the cerebrum and the minimum value was the half-value of the mean pixel value of the gray matter (center of the caudate head) and the mean value of the cerebral spinal fluid (CSF) (center of the lateral ventricle). The slice volume of each structure was obtained by automatically counting the number of pixels within the segmented regions and then multiplying it by a voxel size ($220/2562 \times 1.5 = 1.1078$ mm^3).

Boundaries for the hippocampal formation and parahippocampal gyrus were defined as follows: The hippocampal formation was included the pes hippocampi, digitations hippocampi, alveus hippocampi, dentate gyrus and subiculum. The most posterior boundary was the plane intersecting the portion where the pes of the folnix arises. The outline boundary was manually guided along the hippocampal sulcus, medially to inferior horn of the lateral ventricle and turned up laterally along the choroidal fissure (*12,25,27*). Anteriorly, the disarticulation of the hippocampal formation head was arbitrarily separated from the amygdala as a marker of the alveus hippocampi, the semianular (amygdaloid) sulcus or the uncal recess of inferior horn of the lateral ventricle (*27*). The parahippocampal gyrus included the parahippocampal gyrus proper, entorhinal cortex and their underlying white matter (*26*). The posterior boundary for the parahippocampal gyrus was the plane intersecting the posterior commissure as for the hippocampal formation. The anterior boundary was the plane including the most anterior part of the temporal stem. The outline boundary was drawn along the hippocampal sulcus and medially to the inferior horn of the lateral ventricle, turning down laterally to the collateral sulcus. Anteriorly, the superior-medial border of the parahippocampal gyrus was covered by a medio-inferior part of the amygdala. At this level, disarticulation of the parahippocampal gyrus was arbitrarily made by drawing a line from the tentorial indentation (uncal notch) to the inferior horn of the lateral ventricle.

Statistical Analysis

Two-way analysis of variance (ANOVA), or one-way ANOVA when cross-reactivity exists, and posthoc Scheffé's test was performed to detect regional differences between the Alzheimer's disease and control groups. Pearson correlation was used to test the relationship between blood flow/metabolism and volume of the each medial temporal structure and the relationship between blood flow/metabolism and cognitive function. Criterion for statistical significance was a p-value less than 0.05.

RESULTS

In every region, decline of $CMRO_2$ in the Alzheimer's disease group was greater than that of CBF. The mean $CMRO_2$ in the medial temporal, lateral temporal cortex and parietal cortex was significantly lower in the patient group than in the control group. The mean CBF in the parietal and lateral temporal cortices was also significantly lower in the patient group than in the control group. For the medial temporal lobe, the mean $CMRO_2$ in the Alzheimer's disease group significantly decreased to 76.7% of that of the control group, while the mean CBF in the Alzheimer's disease group decreased to 87.0% of that of the control group. The difference between the two groups did not reach a significant level (Table 2, Fig. 2). For the parietal and lateral temporal cortices, both $CMRO_2$ and CBF were significantly decreased compared with the control group. In OEF, repeat two-way ANOVA showed significant group x region interaction ($F[4, 112] = 2.89$; $p = 0.0255$). One-way ANOVA revealed a significant difference among regional OEF in the Alzheimer's disease group and the control group ($F[9, 140] = 4.68$; $p = 0.0001$). The medial temporal OEF was significantly lower compared with other cortical regions, and the medial temporal OEF in the Alzheimer's disease group was significantly lower than that of control group ($p < 0.05$), which indicated that medial temporal OEF in the Alzheimer's disease group was severely reduced. There were no significant regional CBV differences between the Alzheimer's disease and control groups. For the cerebellum, there were no significant differences in CBF, $CMRO_2$, OEF and CBV between the two groups.

Figure 3 demonstrates typical CBF and $CMRO_2$ images in a normal control subject. There were no abnormal reductions of perfusion and oxygen metabolism. Moreover, the medial temporal $CMRO_2$ was intact. Figure 4 shows the PET images in a patient with Alzheimer's disease, in which both CBF and $CMRO_2$ were characteristically decreased in the medial temporal, lateral temporal, frontal and parietal temporal regions, while those in the primary visual and sensorimotor cortices were preserved. A few patients had decreased $CMRO_2$ in the medial temporal lobe with unaffected CBF and had preserved CBF and $CMRO_2$ in other cortical regions (Fig. 5).

Table 3 summarizes the results of medial temporal volumetry. The mean volume of hippocampal formation in the Alzheimer's disease group was 82.8% of that of the control group and the difference was significant. The mean parahippocampal gyrus volume in the Alzheimer's disease group was 87.8% of that of the control group. Medial temporal CBF and $CMRO_2$ were not correlated with the hippocampal formation, parahippocampal gyrus and medial temporal lobe volumes either in the Alzheimer's disease group or in the control group (Table 4).

Correlations between cognitive or memory test scores and medial temporal CBF or $CMRO_2$ in Alzheimer's disease are summarized in Table 5. Although the absolute value of medial temporal CBF or $CMRO_2$ did not correlate with any of these scores, when normalized for individual differences in blood flow and oxygen metabolism (the value of each medial tempo-

TABLE 2
Mean rCBF and Oxygen Metabolism in Alzheimer's Disease Patients and Normal Control Subjects

	Med. temp.	Lat. temp.	Occipital	Frontal	Parietal	Cerebellum
CBF						
Alzheimer's disease	41.1 ± 10.0	45.5 ± 13.3*	61.4 ± 11.8	48.3 ± 15.3	41.5 ± 11.8*	88.3 ± 21.3
Control	47.2 ± 8.3	54.1 ± 7.5	65.1 ± 11.8	53.4 ± 8.5	50.5 ± 8.6	87.1 ± 19.1
Reduction ratio†	87.0%	84.1%	94.3%	90.4%	82.2%	101.4%
$CMRO_2$						
Alzheimer's disease	2.04 ± 0.42†	3.08 ± 0.75*	3.85 ± 0.71	3.12 ± 0.84	2.79 ± 0.69†	5.46 ± 2.03
Control	2.66 ± 0.42	3.68 ± 0.49	4.26 ± 0.66	3.54 ± 0.46	3.48 ± 0.62	5.52 ± 1.22
Reduction ratio‡	76.7%	83.7%	90.3%	88.1%	80.1%	98.9%
OEF						
Alzheimer's disease	32.0 ± 6.4*	40.8 ± 7.1	40.3 ± 5.9	40.6 ± 6.7	42.7 ± 6.6	37.2 ± 6.7
Control	35.2 ± 5.7	42.2 ± 6.5	42.0 ± 6.0	41.6 ± 6.3	42.4 ± 6.7	39.9 ± 7.0
CBV						
Alzheimer's disease	6.92 ± 2.52	6.57 ± 2.14	7.65 ± 2.10	5.35 ± 2.08	5.39 ± 2.22	7.40 ± 2.90
Control	7.18 ± 1.73	6.46 ± 2.16	7.50 ± 2.03	5.43 ± 1.72	5.62 ± 1.89	7.43 ± 2.82

*$p < 0.05$, †$p < 0.01$.
†mean CBF of Alzheimer's disease group/mean CBF of control group.
‡mean $CMRO_2$ of Alzheimer's disease group/mean $CMRO_2$ of control group.
Values are mean ± 1 s.d. Med. temp. = medial temporal lobe; Lat. temp. = lateral temporal lobe; CBF = cerebral blood flow (ml/100 ml/min); $CMRO_2$ = cerebral metabolic ratio for oxygen (ml/100 ml/min); OEF = oxygen extraction fraction (%); CBV = cerebral blood volume (ml/100 ml).

ral structure was divided by the value of the cerebellar cortices), the medial temporal CBF and $CMRO_2$ significantly correlated with visual paired associates and visual reproduction. The medial temporal $CMRO_2$ correlated with Mini-Mental State Examination and Alzheimer's Disease Assessment Scale scores.

DISCUSSION

In this study, we measured oxygen metabolism at baseline in the medial temporal lobe and found it to be relatively high compared to that of the glucose metabolic rate (*28,29*). We identified metabolic involvement in the medial temporal lobe, including the hippocampus and parahippocampal gyrus in patients with mild-to-moderate Alzheimer's disease, as a decrease of oxygen metabolism. We also noted declines in oxygen metabolism and regional blood flow in the lateral temporal and parietal cortices, which supports the findings of previous studies (*3, 9*). In Alzheimer's disease, oxygen metabolism and regional blood flow in the medial temporal lobe, when normalized for individual differences, correlated with some of the nonverbal memory test scores (visual paired associates and visual reproduction) and cognitive impairment scales.

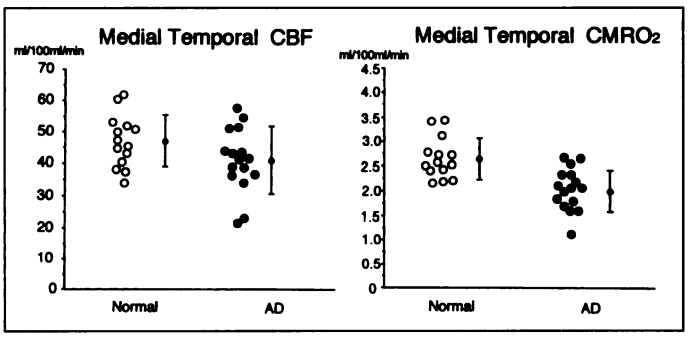

FIGURE 2. Medial temporal CBF and $CMRO_2$ in the control and Alzheimer's disease groups. There was a significant difference in the medial temporal $CMRO_2$ between the two groups but not in the CBF.

When interpreting PET images, especially when measuring small structures surrounded by quite different tissues (i.e., medial temporal lobe) partial volume effects have to be considered. Because the medial temporal lobe is surrounded by CSF, in which there is no blood flow metabolism, the partial volume effect may be more critical when the structure is reduced in size. In the present study, however, ROI measurements were independent of each medial temporal structure's volume. The mean hippocampal and parahippocampal volume reductions in the Alzheimer's disease group were 17.2% and 12.2%, respectively, compared to the control group, which can be calculated as 6.1% and 4.2% reductions in each dimension. These data suggest that partial volume effects are unlikely to affect ROI measurements. Furthermore, the mean medial temporal CBV was identical between patients and controls. If the ROI had contained significant amounts of CSF, then CBV (i.e., the volume of the vascular bed in a unit volume) would have decreased. Therefore, partial volume effects, involved the ROI

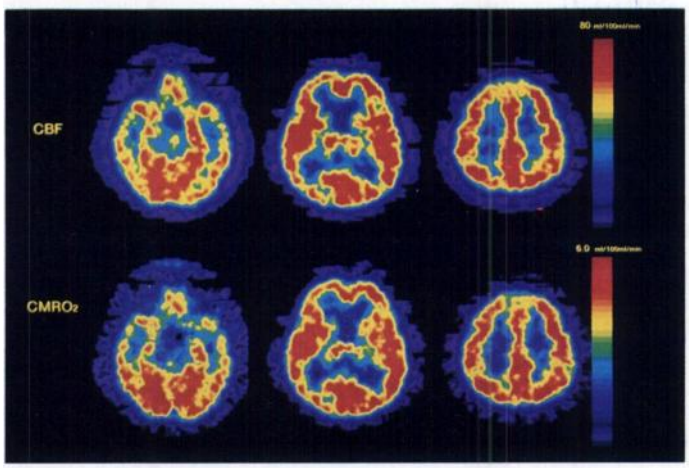

FIGURE 3. PET studies in a 63-yr-old normal volunteer demonstrate no abnormal findings in either the CBF or $CMRO_2$ images.

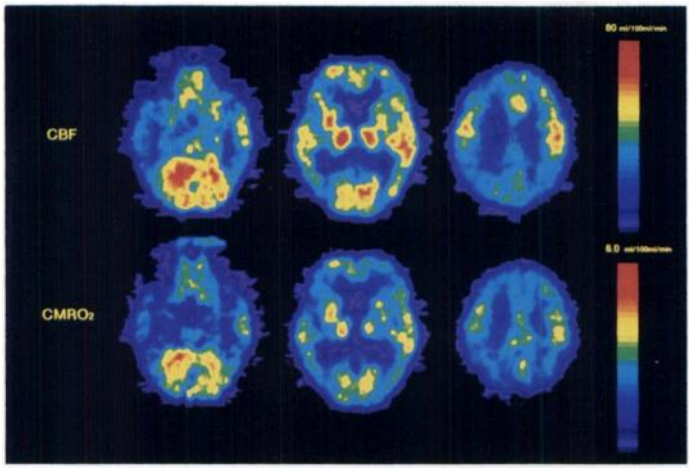

FIGURE 4. PET studies of an Alzheimer's disease patient. Both CBF and $CMRO_2$ in the parietal lobe were decreased. Medial temporal CBF and $CMRO_2$ were also decreased.

measurements of each group evenly, and the medial temporal hypoperfusion and hypometabolism in this series of Alzheimer's disease patients could not be attributable to their volume reduction but reflects the pathophysiological changes in the medial temporal lobe in Alzheimer's disease.

Interestingly, in normal subjects, the medial temporal OEF was lower than that of other cortical regions. As our results indicate, this might be attributed to cytoarchitecture of cortices; the medial temporal regions mainly consist of the limbic system belonging to the archi- and paleocortex and other cortical regions belonging to the neocortex. Vascular beds and metabolism would therefore differ from each other. This disparity might be enhanced by the pathological process of Alzheimer's disease. The mechanism for the uncoupling of CBF and $CMRO_2$ in the medial temporal cortex in Alzheimer's disease remains unknown. One possible explanation is that an impairment of oxygen metabolism precedes a change of cerebral blood flow, which could be designated as a luxury perfusion state. Cerebral blood flow might not parallel the decline of oxygen demand in the medial temporal lobe in early Alzheimer's disease.

The medial temporal lobe, especially the hippocampus and entorhinal cortex, plays a crucial role in memory function. Damages in this area causes memory impairment in animals and humans. In Alzheimer's disease patients, MR volumetric studies demonstrate correlation between hippocampal atrophy and

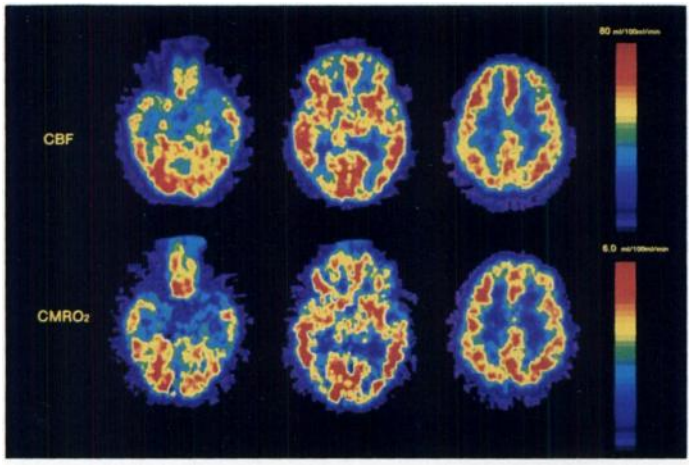

FIGURE 5. PET studies of an Alzheimer's disease patient. Medial temporal $CMRO_2$, but not CBF, was decreased. Both parietal CBF and $CMRO_2$ were preserved.

TABLE 3
Mean Volumes of Hippocampus and Hippocampus/Parahippocampal Gyrus in Alzheimer's Disease Patients and Normal Control Subjects

Group	HF	PHG	MTL
Alzheimer's disease	2.03 ± 0.53cm³*	3.80 ± 0.71cm³	5.83 ± 1.10cm³*
Control	2.45 ± 0.42 cm³	4.33 ± 8.3 cm³	6.78 ± 1.13 cm³
Reduction ratio†	82.8%	87.8%	86.1%

*$p < 0.05$.

†mean volume of Alzheimer's disease group/mean volume of control group.

HF = hippocampal formation; PHG = parahippocampal gyrus; MTL = medial temporal lobe = HF + PHG.

Volume of each structure (mean ± s.d.) is shown as the average of the right and left volumes.

the severity of memory impairment. Although Ohnishi et al. (*15*) in their ^{99m}Tc-HMPAO SPECT study found that hippocampal "hypoperfusion" correlated with cognitive decline in amnesia patients, including those with Alzheimer's disease, the effect of atrophy on their results was immeasurable. The present study found correlation between certain types of memory function and medial temporal oxygen metabolism in Alzheimer's disease, when individual difference of oxygen metabolism was normalized. Our results provide an important clue for PET studies of memory impairment, and involvement of the medial temporal lobe and other cites relevant to human memory function should also be examined in various causes of amnesia.

Finally, the present finding of significantly decreased oxygen metabolism in the medial temporal lobe has considerable effect on the diagnosis of Alzheimer's disease. Medial temporal oxygen hypometabolism would be more accurate than parietal or parietotemporal hypoperfusion/glucose hypometabolism in the diagnosis of early Alzheimer's disease. The clinical role of oxygen metabolism measurement may be limited so far, since functional imaging with PET is still largely a research tool and measurement of oxygen metabolism by SPECT has not yet been developed. Nevertheless, as high-resolution scanners and tracers such as ^{99m}Tc-ethyl cycteinate dimer (*30*) appear that may correlate with oxygen metabolism, the value of SPECT in showing medial temporal involvement and its role in diagnosis of early Alzheimer's disease would be encouraging. In SPECT studies, hippocampal atrophy in Alzheimer's disease may largely obscure the true pathophysiological changes (i.e., $CMRO_2$ reduction). However, the results affected by partial volume effects may reflect both pathophysiological and structural changes and may be practical in clinical use.

TABLE 4
Correlations Between Medial Temporal CBF/$CMRO_2$ and Temporal Structure Volumes

Group	HF	PHG	MTL
Alzheimer's disease			
CBF	0.260 (p=0.330)	0.069 (p=0.799)	0.172 (p=0.524)
$CMRO_2$	0.018 (p=0.949)	0.282 (p=0.290)	0.192 (p=0.477)
Controls			
CBF	0.008 (p=0.978)	0.097 (p=0.740)	0.068 (p=0.816)
$CMRO_2$	0.494 (p=0.073)	0.398 (p=0.159)	0.478 (p=0.084)

HF = hippocampal formation; PHG = parahippocampal gyrus; MTL = medial temporal lobe (HF and PHG).

TABLE 5
Pearson Correlations between MMSE/ADAS Sores/Wechsler Memory Scale Revised Test Scores and Medial Temporal CBF/$CMRO_2$

Test	Medial temporal CBF	Medial temporal $CMRO_2$	Normalized medial temporal CBF	Normalized medial temporal $CMRO_2$
MMSE	0.218 (p = 0.418)	0.084 (p = 0.758)	0.341 (p = 0.197)	0.603 (p = 0.014)
ADAS	−0.249 (p = 0.353)	−0.365 (p = 0.164)	−0.112 (p = 0.679)	−0.546 (p = 0.029)
ADAS recall	−0.064 (p = 0.825)	0.390 (p = 0.151)	−0.361 (p = 0.186)	0.005 (p = 0.987)
Figural memory	−0.196 (p = 0.484)	0.078 (p = 0.783)	0.262 (p = 0.349)	0.355 (p = 0.194)
Logical memory	−0.242 (p = 0.385)	0.146 (p = 0.605)	−0.038 (p = 0.893)	0.253 (p = 0.363)
Visual paired associates	0.271 (p = 0.328)	−0.078 (p = 0.752)	0.582 (p = 0.023)	0.554 (p = 0.032)
Verbal paired associates	0.112 (p = 0.691)	0.305 (p = 0.269)	0.210 (p = 0.452)	0.143 (p = 0.612)
Visual reproduction	0.214 (p = 0.444)	−0.176 (p = 0.531)	0.596 (p = 0.019)	0.564 (p = 0.028)

Normalized medial temporal CBF = CBF ratio of medial temporal lobe versus cerebellum.
Normalized medial temporal $CMRO_2$ = $CMRO_2$ ratio of medial temporal lobe versus cerebellum.

CONCLUSION

We used an ^{15}O steady-state method and PET to demonstrate medial temporal involvement in patients with mild-to-moderate Alzheimer's disease. In the medial temporal lobe, reduction of $CMRO_2$ was evident with relatively preserved CBF and decreased OEF. An MRI volumetric study of the medial temporal structures indicated that these measurements were not attributed to partial volume effect as a result of atrophy but rather reflect the pathophysiological changes in Alzheimer's disease and the unique cytoarchitecture of the medial temporal lobe. These results substantiate the functional impairment of the medial temporal region in Alzheimer's disease and suggest the clinical significance of medial temporal metabolic and perfusion changes in the diagnosis of early Alzheimer's disease.

ACKNOWLEDGMENTS

We thank Dr. C. Tanaka (Director, Hyogo Institute for Aging Brain and Cognitive Disorders[HI-ABCD]) for her continuous encouragement and critical review of the manuscript. We also thank Drs. M. Sasaki, S. Sakamoto and S. Yamaji (Division of Neuroimaging Research, HI-ABCD) for their assistance in performing the PET scans; and Drs. N. Hirono, Y. Ikejiri, T. Imamura, T. Shimomura, M. Ikeda and H. Yamashita (Division of Clinical Neurosciences, HI-ABCD) for their support and for providing clinical information. Lastly, we thank T. Kida, RT and H. Sakai, RT, (Radiology Service, HI-ABCD) for their technical support.

REFERENCES

1. Brun A, Englund E. Regional pattern of degeneration in Alzheimer's disease: neuronal loss and histopathological grading. *Histopathol* 1981;5:549–564.
2. Coleman PD, Flood DG. Neuron numbers and dendritic extent in normal aging and Alzheimer's disease. *Neurobiol Aging* 1987;8:521–545.
3. Frackowiak RSJ, Pozzilli C, Legg NJ, et al. Regional cerebral oxygen supply and utilization in dementia. A clinical and physiological study with oxygen-15 and positron tomography. *Brain* 1981;104:753–778.
4. Nybäck H, Nyman H, Blomqvist G, Sjögren I, Stone-Elander S. Brain metabolism in Alzheimer's dementia: studies of ^{11}C-deoxyglucose accumulation, CSF monoamine metabolites and neuropsychological test performance in patients and healthy subjects. *J Neurol Neurosurg Psych* 1991;54:672–678.
5. Cutler NR, Haxby JV, Duara R, et al. Clinical history, brain metabolism and neuropsychological function in Alzheimer's disease. *Ann Neurol* 1985;18:298–309.
6. Friedland RP, Brun A, Budinger TF. Pathological and positron emission tomographic correlation in Alzheimer's disease. *Lancet* 1985;1:228.
7. Jagust WJ, Seab JP, Huesman RH, et al. Diminished glucose transport in Alzheimer's disease: dynamic PET studies. *J Cereb Blood Flow Metab* 1991;11:323–330.
8. Bonnte FJ, Tintner R, Weiner MF, Bigino EH, White III CL. Brain blood flow in the dementias: SPECT with histopathologic correlation. *Radiology* 1993;186:361–365.
9. Holman BL, Johnson KA, Gerada B, Carvalho PA, Satlin A. The scintigraphic appearance of Alzheimer's disease: a prospective study using technetium-99m-HMPAO SPECT. *J Nucl Med* 1992;33:181–185.
10. Fukuyama H, Ogawa M, Yamauchi H, et al. Altered cerebral energy metabolism in Alzheimer's disease: a PET study. *J Nucl Med* 1994;35:1–6.
11. Powers WJ, Perlmutter JS, Videen, et al. Blinded clinical evaluation of positron emission tomography for diagnosis of probable Alzheimer's disease. *Neurology* 1992;42;765–770.
12. Jack CR Jr, Petersen RC, O'brien PC, Tangalos EG. MR-based hippocampal volumetry in the diagnosis of Alzheimer's disease. *Neurology* 1992;42:183–188.
13. Press GA, Amaral DG, Squire LR. Hippocampal abnormalities in amnesic patients revealed by high-resolution magnetic resonance imaging. *Nature* 1989;341:54–57.
14. Ikeda M, Tanabe H, Nakagawa Y, et al. MRI-based quantitative assessment of the hippocampal region in very mild-to-moderate Alzheimer's disease. *Neuroradiology* 1994;36:7–10.
15. Ohnishi T, Hoshi H, Nagamachi S, et al. High-resolution SPECT to assess hippocampal perfusion in neuropsychiatric diseases. *J Nucl Med* 1995;36:1163–1169.
16. Frackowiak RSJ, Lenzi GL, Jones T, Heather JD. Quantitative measurement of regional cerebral blood flow and oxygen metabolism in man using ^{15}O and positron emission tomography: theory, procedure and normal values. *J Comput Assist Tomogr* 1980;4:727–736.
17. McKhann G, Drachman D, Folstein M, Katzman R, Price D, Stadlan EM. Clinical diagnosis of Alzheimer's disease: report of the NINCDS-ADRDA Work Group under the auspices of Department of Health and Human Services Task Force on Alzheimer's disease. *Neurology* 1984;34:939–944.
18. Berg L. Clinical dementia rating. *Psychopharmacol Bull* 1988;24:637–639.
19. Mori E, Mitani Y, Yamadori A. Usefulness of Japanese version of the Mini-Mental State test in neurological patients. *Jpn J Neruopsychiatry* 1985;1:82–90.
20. Honma A, Fukuzawa K, Tsukada Y, Ishii T, Hasegawa K, Mohs RC. Development of a Japanese version of Alzheimer's Disease Assessment Scale. *Jpn J Geriatr Psychiatry* 1992;3:647–655.
21. Wechsler D. Wechsler memory scale revised manual. San Antonio: Harcourt Brace Jovanovich, 1987.
22. Iida H, Miura S, Kanno I, et al. Design of evaluation of Headtome IV: a whole-body positron emission tomograph. *IEEE Trans Nucl Sci* 1989;NS-37:1006–1010.
23. Talairach J, Tournoux P. *Co-planar stereotaxic atlas of the human brain.* Stuttgart: Thieme-Verlag; 1988.
24. Lammertsma AA, Jones T. Correction for the presence of intravascular oxygen-15 in the steady state technique for measuring regional oxygen extraction ratio in the brain: I. Description of the method. *J Cereb Blood Flow Metab* 1983;3:416–424.
25. Jack CR Jr, Twomey CK, Zinsmeister AR, Sharbrough FW, Petersen RC, Cascino GD.

Anterior temporal lobes and hippocampal formations: normative volumetric measurements from MR images in young adults. *Radiology* 1989;172:549–554.
26. Yoneda Y, Mori E, Yamashita H, Yamadori A. MRI volumetry of medial temporal lobe structures in amnesia following herpes simplex encephalitis. *Eur Neurol* 1994; 34:243–252.
27. Watson C, Andermann F, Gloor P, et al. Anatomic basis of amygdaloid and hippocampal volume measurement by magnetic resonance imaging. *Neurology* 1992; 42:1743–1750.
28. Duara R, Grady C, Haxby J, et al. Human brain glucose utilization and cognitive function in relation to age. *Ann Neurol* 1984;16:702–713.
29. Yamaguchi T, Kanno I, Uemura K, et al. Reduction in regional cerebral metabolic rate of oxygen during human aging. *Stroke* 1986;17:1220–1228.
30. Tsuchida T, Nishizawa Y, Yonekura Y, et al. SPECT images of technetium-99m-ethyl cysteinate dimer in cerebrovascular disease: comparison with other cerebral perfusion tracers and PET. *J Nucl Med* 1994;35:27–31.

(continued from page 5A)

FIRST IMPRESSIONS:
Brain SPECT with Cortical Photopenic Defect

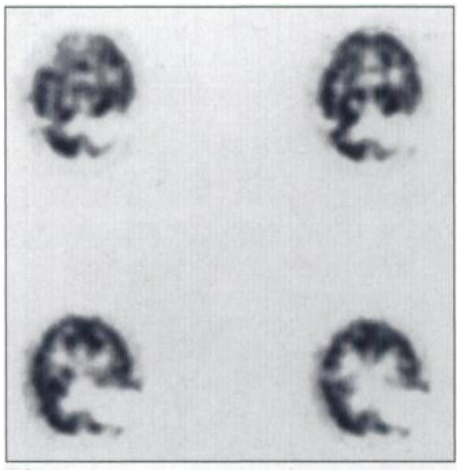

Figure 1.

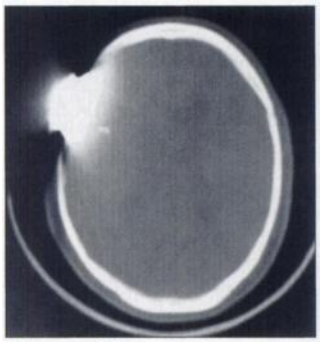

Figure 2.

Figure 3.

PURPOSE
A 71-yr-old man with a history of mild CVA in 1990 presented with clinical dementia. The patient was referred for brain SPECT imaging to rule out Alzheimer's disease. Figure 1 shows axial images of the brain with a round photopenic defect in the right frontal lobe that extends outside the cortex and into the cranium and soft tissues. Figures 2 and 3 depict axial CT images through the metal plate and a digital lateral skull film with the metal plate clearly demonstrated.

TRACER
Technetium-99m-HMPAO, 32 mCi (884 MBq)

ROUTE OF ADMINISTRATION
Intravenous

TIME AFTER INJECTION
90 minutes

INSTRUMENTATION
Picker Triple-Head Prism 3000 SPECT with ultra-high resolution, fanbeam collimation

CONTRIBUTORS
Edwin L. Boren, Jr., Christopher L. Cowan and Shirley G. Anderson

INSTITUTION
John L. McClellan Memorial Veterans Hospital, Little Rock, Arkansas